JAST, Vol. 3, No. 3, pp 125–133

JAST
Journal of Aerospace Science and Technology

In-Trim Flight Investigations of a Conceptual Fluidic Thrust-Vectored Unmanned Tail-Sitter Aircraft

F. Saghafi[1], A. Banazadeh[2]

The feasibility of using a stand alone Fluidic Thrust-Vectoring (FTV) system for the purpose of longitudinal trim of an unmanned aerial vehicle is the focus of the research presented in this paper. Since the fluidic thrust vectoring requires high pressure secondary air to deflect the engine exhaust gases, this research also provides an analytical toolset for the preliminary sizing of a suitable secondary air supply. The study is based on a conceptual model of a Vertical Take-Off and Landing (VTOL) Tail-sitter type unmanned aerial vehicle in three common phases of flight named as Hovering, Transition and Cruise. A relationship is finally presented between the thrust-vectoring angle and the required secondary mass flow rate.

It is found that, just by use of FTV system the aircraft trim is possible. In addition, the mathematical model developed in this study can be used as a preliminary tool for overall performance evaluation of such a conceptual aircraft, especially for sensitivity analysis of thrust-vectoring control and finding the optimum values of the parameters like centre of gravity and engine location.

NOMENCLATURE

M	Mach number
C_L, C_D, C_Y	Lift, drag and side force coefficients
C_l, C_m, C_n	Rolling, pitching and yawing moment coefficients
$\bar{c}, b$	Wing chord and span (m)
α	Angle of attack (rad)
β	Angle of sideslip (rad)
p, q, r	Roll, pitch and yaw rates (rad/s)
u, v, w	Velocity components (m/s)
$I_{xx}, I_{yy}, I_{zz}, I_{xy}, I_{xz}, I_{yz}$	Moments of inertia
ψ, θ, ϕ	Euler angles (rad)
$\bar{q}$	Dynamic pressure (N/m^2)
m	Aircraft mass (kg)
L, M, N	Moment components (Nm)
f_x, f_y, f_z	Force components (N)
$C_{\frac{w}{b}}$	Wind to body transformation matrix
P_N, P_E, h	Position components (m)
m_i	Moment vector
α_T, β_T	Thrust vectoring angles (rad)
T	Engine thrust (N)
X_T, Y_T, Z_T	Components of thrust position vector (m)
ρ	Air density (Kg/m^3)
γ	Flight path angle (rad)
r	Thrust position vector
ω	Angular velocity vector
V_T	Translational velocity (m/s)

Subscript

a	Aerodynamic
p	Propulsion
L	Left
R	Right

1. *Assistant Professor, Dept. of Aerospace Eng., Sharif Univ. of Tech., Tehran, Iran, Email: saghafi@sharif.edu.*
2. *Ph.D. Candidate, Dept. of Aerospace Eng., Sharif Univ. of Tech., Tehran, Iran.*

e	Earth
b	Body
$C.G.$	Centre of Gravity

Superscript

B	Body coordinate system
T	Transpose
$\dot{x}$	Time rate of change of parameter x

INTRODUCTION

An unmanned aerial vehicle (UAV) is a remotely controlled or autonomous aircraft that has shown a great potential of usage in different applications for the 21st century. One class of UAVs, called Vertical Take-Off and Landing (VTOL) UAVs, has the ability of independent vertical take-off and landing like helicopters and at the same time fly horizontally like fixed wing aircraft. These abilities are important from the operational point of view and are considered as a great advantage for a UAV.

Tilt-rotors, Tilt-bodies and Tail-sitters are three proven concepts of VTOL UAV configurations, in all of which the propulsion system is of rotor/propeller type [1-4]. As an inherent characteristic, this kind of propulsion system is not suitable for high speed flight in which the wave drag increases rapidly in the tip of rotors/propellers. Tilt-rotors and Tilt-bodies also suffer significant extra mechanical complexity with their related maintenance problems and weight penalties in comparison with Tail-sitters which have a simple configuration with a fixed wing, body and nacelles.

To have a VTOL UAV with minimum mechanical complexity and maximum flight speed, a jet-propelled tail-sitter UAV could be a good candidate. However, elimination of propellers and in turn their slipstreams over control surfaces which play an important role for tail-sitter stabilization in hovering, early vertical to horizontal and late horizontal to vertical transition modes [5,6], should be somehow compensated. The compensation could be carried out by using a jet thrust vectoring system either mechanically or fluidic (Figure 1). Mechanical thrust vectoring designs are often heavy, complex, expensive, and counter-productive to stealth requirements. Fluidics, however, offer reduced weight, higher reliability, and stealth compatibility [7-11].

In this study a conceptual model of a micro-jet engine tail-sitter aircraft is considered with a co-flow fluidic type thrust vectoring system that uses high pressure secondary air and Coanda surface to deflect the engine thrust. This integrated system is then analyzed in different modes of flight in order to evaluate the feasibility of the concept.

It should be pointed out that even for a conventional aircraft (without the VTOL ability), thrust vectoring can significantly improve the aircraft design characteristics and performance. For this reason, thrust vectoring seems to be headed towards greatly expanded use in the next generation of UAVs [12-14].

CONCEPTUAL THRUST-VECTORING UNMANNED TAIL-SITTER (CTUT) AIRCRAFT

CTUT is a Conceptual Thrust vectoring Unmanned Tail-sitter aircraft planned as a preliminary proof-of-the-concept demonstrator. The CTUT configuration characteristics are chosen among some of the unmanned aerial targets such as Banshee, Crecerelle and Tasuma MMT100 [2, 3], regarding the following points:

- Utilization of thrust vectoring benefits
- Foresight strategies in the next UAV generations
- Simplicity and data availability
- Microjet engine/airframe integration programs
- Manufacturing feasibility and simplicity

Discussing the whole configuration design process and related decision makings, regarding the engine airframe integration, is beyond the scope of this work. Therefore, only the major finalized aircraft characteristics are given in Tables 1 and 2. The CTUT final configuration is schematically shown in Figure 2.

It is assumed that FTV is also achievable by using any of the secondary air supply options such as: compressed air tank, engine compressor bleeding or additional electrically driven compressor.

The performance, stability and control characteristics of an aircraft depend on the aerodynamic forces and moments acting on it, and in turn on its aerodynamic derivatives. These derivatives depend on the shape, velocity, and attitude of the vehicle. The CTUT aerodynamic derivatives are derived using a commercially available software in three flight speed

Table 1. CTUT General Characteristics.

Reference Area	2 m^2
Take off mass	46 kg
Mean Aerodynamic Chord	1.02 m
Wing Span	2.2 m
$X_{C.G.}$ from Trailing Edge	0.78 m
$X_{T.V.}$ from C.G.	0.91 m
$Y_{T.V.}$ from C.G.	0.25 m

Table 2. General Characteristics of CTUT Engine.

Maximum RPM	108,000
Thrust @ Max. RPM	190 N
Fuel Consumption @ Max. RPM	640 gr/min
Dimensions	130 × D375 L mm
Weight	2.85 kg

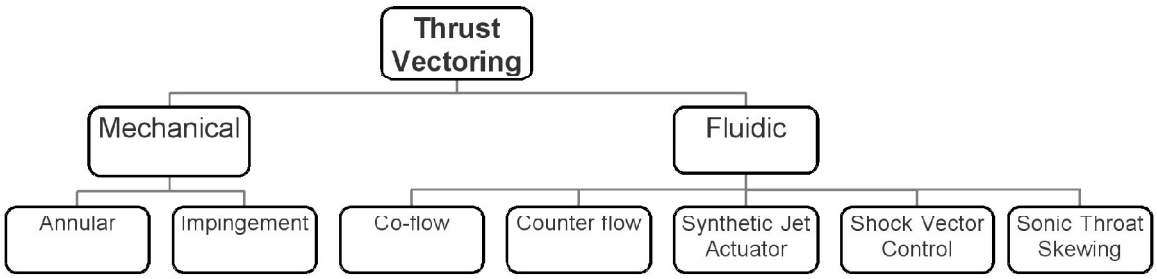

Figure 1. Thrust vectoring systems.

regimes, $M < 0.185$, $0.185 \leq M \leq 0.3$ and $0.3 < M$. Since CTUT is a low subsonic vehicle, there is no need to calculate derivatives in speed regimes more than $M = 0.7$. It is also assumed that flight altitude is less than 5000 ft. Therefore, only three sets of derivatives corresponding to the given ranges of mach numbers are sufficient to cover the whole flight envelope including three defined phases of flight. The most important derivatives are highlighted in Table 3 and the other derivatives are supposed to be negligible regarding the flight conditions and aircraft configuration.

AIRCRAFT SIMULATION

In order to construct the aircraft simulation, the governing equations of motion are formulated to obtain the mathematical model. The simulation method is based on Cartesian approach that formulates the equations in Cartesian coordinates. The aerodynamic derivatives are calculated in the stability or wind axis system regarding the negligible angle of sideslip. Therefore, the

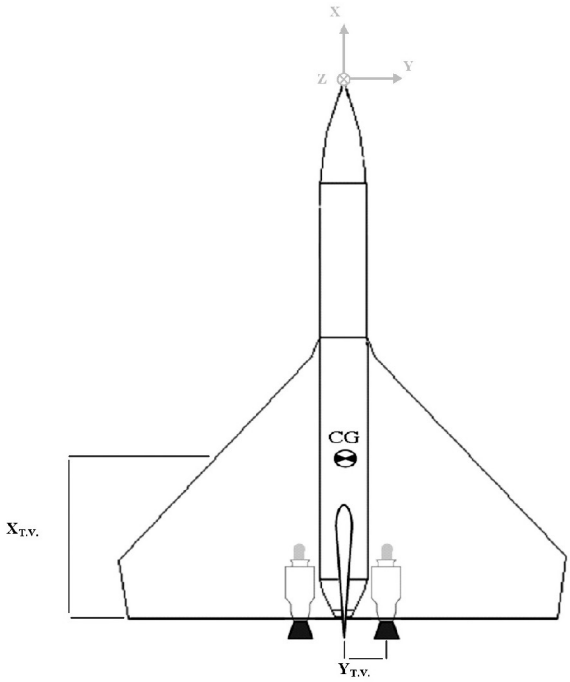

Figure 2. Schematic configuration of CTUT

Table 3. CTUT whole derivatives and the most important ones.

$\mathbf{C_L}$	$\mathbf{C_{L0}}$	$\mathbf{C_{L\alpha}}$	$C_{L\dot{\alpha}}$	$\mathbf{C_{Lq}}$	C_{Lu}	$\mathbf{C_{L\delta}}$
$\mathbf{C_D}$	$\mathbf{C_{D0}}$	$\mathbf{C_{D\alpha}}$	$C_{D\dot{\alpha}}$	C_{Dq}	C_{Du}	$C_{D\delta}$
$\mathbf{C_m}$	$\mathbf{C_{m0}}$	$\mathbf{C_{m\alpha}}$	$C_{m\dot{\alpha}}$	$\mathbf{C_{mq}}$	C_{mu}	$C_{m\delta}$
$\mathbf{c_l}$	c_{l0}	$\mathbf{c_{l\beta}}$	$c_{l\dot{\beta}}$	$\mathbf{c_{lp}}$	$\mathbf{c_{lr}}$	$c_{l\delta}$
$\mathbf{c_n}$	c_{n0}	$\mathbf{c_{n\beta}}$	$c_{L\dot{\beta}}$	$\mathbf{c_{np}}$	$\mathbf{c_{nr}}$	$c_{n\delta}$
$\mathbf{c_y}$	c_{y0}	$\mathbf{c_{y\beta}}$	$c_{y\dot{\beta}}$	$\mathbf{c_{yp}}$	c_{y_r}	$c_{y\delta}$

forces and moments calculated in the wind coordinate system have to be transformed to the body coordinate system using the wind to body transformation matrix. The CTUT equations of motion are derived and assembled as follows using refs. [15-18]. It should be pointed out that the complete 6DOF equations of motion have been derived and programmed for the sake of completeness and the needs for the future studies, whereas for the present work, these equations have only been used to study the in-vertical-plane 3DOF motion of the aircraft.

- Moment Equations

$$I_{XX}\dot{p} - I_{XZ}\dot{r} - I_{XZ}pq + (I_{ZZ} - I_{YY})rq = L_a + L_p$$
$$I_{YY}\dot{q} + (I_{XX} - I_{ZZ})pr + I_{XZ}(p^2 - r^2) = M_a + M_p$$
$$I_{ZZ}\dot{r} - I_{XZ}\dot{p} + (I_{YY} - I_{XX})pq + I_{XZ}qr = N_a + N_p \quad (1)$$

- Force Equations

$$m(\dot{u} - vr + wq) = -mg\sin\theta + f_{aX} + f_{pX}$$
$$m(\dot{v} + ur - wp) = -mg\cos\theta\sin\phi + f_{aY} + f_{pY}$$
$$m(\dot{w} - uq + vp) = mg\cos\theta\cos\phi + f_{aZ} + f_{pZ} \quad (2)$$

- Kinematics Equations

$$\dot{\phi} = p + q\sin\phi\tan\theta + r\cos\phi\tan\theta$$
$$\dot{\theta} = q\cos\phi - r\sin\phi$$
$$\dot{\psi} = (q\sin\phi + r\cos\phi)\sec\theta \quad (3)$$

- Navigation Equations

$$\begin{aligned}\dot{P}_N &= u\cos\theta\cos\psi + v\left(-\cos\phi\sin\psi + \sin\phi\sin\theta\cos\psi\right)\\ &\quad + w\left(\sin\theta\sin\psi + \cos\phi\sin\theta\cos\psi\right)\\ \dot{P}_E &= u\cos\theta\sin\psi + v\left(\cos\phi\cos\psi + \sin\phi\sin\theta\sin\psi\right)\\ &\quad + w\left(-\sin\phi\cos\psi + \cos\phi\sin\theta\sin\psi\right)\\ \dot{h} &= u\sin\theta - v\sin\phi\cos\theta - w\cos\phi\cos\theta \end{aligned} \tag{4}$$

where the formatting of force and moment coefficients are in the body coordinates with the positive sense following the direction of the body axes, Figure 3, and:

$$[f_{a,p}]^B = \begin{bmatrix} f_{a,p_x} \\ f_{a,p_y} \\ f_{a,p_z} \end{bmatrix} = f_p^B + \bar{q}S \begin{bmatrix} C_X \\ C_Y \\ C_Z \end{bmatrix} \tag{5}$$

$$[m_{a,p}]^B = \begin{bmatrix} L_{a,p_x} \\ M_{a,p_y} \\ N_{a,p_z} \end{bmatrix} = m_p^B + \bar{q}S \begin{bmatrix} b\,C_l \\ b\,C_m \\ b\,C_n \end{bmatrix} \tag{6}$$

Where,

$$\begin{bmatrix} C_X \\ C_Y \\ C_Z \end{bmatrix}^B = C_{\frac{W}{B}}^T \begin{bmatrix} -CD \\ CY \\ -CL \end{bmatrix}^W \tag{7}$$

$$C_{\frac{W}{B}} = \begin{bmatrix} \cos\alpha\cos\beta & \sin\beta & \sin\alpha\cos\beta \\ -\cos\alpha\sin\beta & \cos\beta & -\sin\alpha\sin\beta \\ -\sin\alpha & 0 & \cos\alpha \end{bmatrix} \tag{8}$$

$$\begin{aligned} f_p^B = f_{p_L}^B + f_{p_R}^B &= \begin{bmatrix} T\cos\beta_T\cos\alpha_{T_L} \\ T\sin\beta_T \\ -T\cos\beta_T\sin\alpha_{T_L} \end{bmatrix} \\ &\quad + \begin{bmatrix} T\cos\beta_T\cos\alpha_{T_R} \\ T\sin\beta_T \\ -T\cos\beta_T\sin\alpha_{T_R} \end{bmatrix} \end{aligned} \tag{9}$$

$$\bar{q} = \frac{1}{2}\rho(h)V_T^2\,; \quad V_T = \sqrt{u^2+v^2+w^2} \tag{10}$$

$$\alpha = \tan^{-1}\left(\frac{w}{u}\right)\,; \quad \beta = \sin^{-1}\left(\frac{v}{V_T}\right) \tag{11}$$

where, $T_L = T_R = T$. It is notable that α_T is different for right and left engines but β_T is the same for two engines and the positive direction is according to the right-hand-rule, respecting to the body z-axis, Figure 3.

$$m_p^B = m_{p_L}^B + m_{p_R}^B = r_L \times f_{p_L}^B + r_R \times f_{p_R}^B \tag{12}$$

$$r_L = \begin{bmatrix} -X_T \\ -Y_T \\ Z_T \end{bmatrix}\,; \qquad r_R = \begin{bmatrix} -X_T \\ Y_T \\ Z_T \end{bmatrix} \tag{13}$$

where, X_T, Y_T, Z_T are absolute values and measured from C.G. and,

$$\begin{bmatrix} C_l \\ C_m \\ C_n \end{bmatrix}^B = C_{\frac{W}{B}}^T \begin{bmatrix} C_l \\ C_m \\ C_n \end{bmatrix}^W \tag{14}$$

The implementation of the mathematical model is carried out using Matlab/Simulink simulation environment.

CO-FLOW FLUIDIC THRUST VECTORING

The concept of fluidic thrust vectoring is to deflect the thrust of a jet by using the influence of a second smaller exhaust stream. This secondary flow would typically be injected into or near the primary jet stream and would require few, if any, moving parts. Nozzle weight and complexity would therefore be reduced. The secondary flow may also be used to provide cooling to nozzle surface. FTV systems are lightweight, simple and relatively inexpensive. They are also of fixed geometry. The main challenge with a fluidic system is in creating an efficient one with acceptable control response characteristics.

Co-flow fluidic thrust vectoring system relies on a phenomenon known as the "Coanda Effect", Figure 4. The Coanda effect is the tendency of a fluid, either gaseous or liquid, to follow the convex curvature of a solid boundary. It happens because of reduction of surface pressure due to a vortex action as the liquid passes over the boundary. It is notable that in this way the flow can even be turned through 180^o. This phenomenon was discovered by Thomas Young in 1800 and its outstanding benefits were understood in 1930. By positioning Coanda surface to the rear of the micro-jet engine nozzle and introducing secondary stream of co-flowing air, parallel to the Coanda surface, thrust vectoring can be formed.

In an experiment being conducted presently, a one dimensional pitch axis co-flow fluidic thrust vectoring demonstrator is going to be developed in static condition. At the same time, it is assumed that such a system is integrated into CTUT micro-jet engine, adding no excess weight and changes in mass and inertia. Therefore, the analysis of required thrust vectoring angle and mass flow rate is possible in different flight phases using the aircraft simulation model and the thrust vectoring mathematical model presented later in this paper.

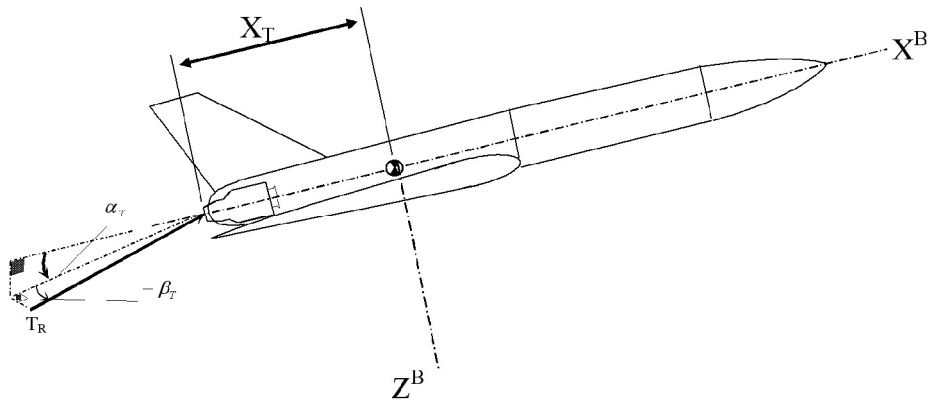

Figure 3. Definitions of the body coordinate axes and thrust vectoring angles.

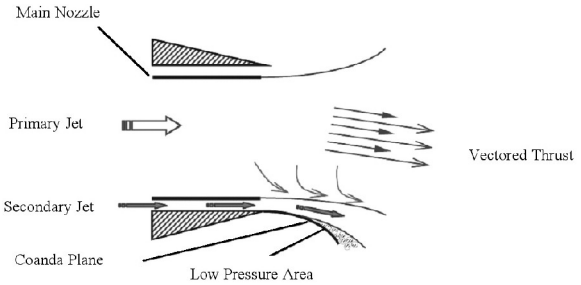

Figure 4. Coanda effect used for Co-Flow FTV

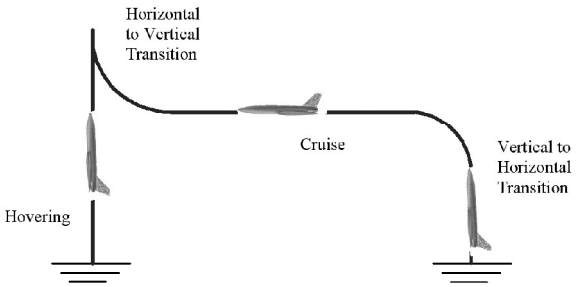

Figure 5. CTUT flight profile.

ANALYSIS OF REQUIRED THRUST VECTORING ANGLE

Analysis of the required thrust vectoring angle is based on trim ability of CTUT in a predefined flight profile, Figure 5. This flight profile is so defined that CTUT first flies from a vertical to a horizontal attitude through a smooth low angle of attack transition. Then, it flies horizontally in cruise mode until it reaches its second transition from horizontal to vertical attitude through a pull-up maneuver to regain a vertical attitude. In this profile, the aircraft velocity changes from zero to a maximum cruise speed and vice versa [19].

Generally, according to the requirements of a steady flight, the known parameters of the previously mentioned mathematical model have been set up for a specific flight condition and the required unknown parameters such as thrust and thrust vectoring angles are obtained by solving trim equations. The trim algorithm is solved using Matlab FSOLVE function by minimizing an error term. The results are presented in the following sections.

NEAR HOVERING AND VERTICAL TO HORIZONTAL (VTH) TRANSITION CLIMB TRIM RESULTS

In this phase the aircraft flies from a zero speed in vertical attitude to a minimum cruise speed in horizontal attitude. A predefined trajectory is assumed in terms of the flight speed and flight path angle as known parameters. The required thrust, thrust vectoring angle, pitch angle and angle of attack (AOA) are then calculated. The obtained results have been tabulated in Table 4. As mentioned before, the flight altitude does not have any noticeable effect on the dynamics of the aircraft in the considered flight profile.

The results shown in Table 4 are an indication of the aircraft ability to climb steadily in various speeds and flight path angles with the required thrust vectoring angles less than 24 degrees. The minus sign of the thrust vectoring angles shows that the required trim moment generated by thrust vectoring is in the pitch up direction. This is an evidence of the static stability tendency of CTUT. In addition, the trim angles of attack are less than 16 degrees, satisfying the assumptions of linearity of the aerodynamic model and low angle of attack flight.

CRUISE TRIM RESULTS

In this phase, the aircraft is supposed to fly steadily in a range of minimum to maximum cruise speeds with zero flight path angles. The required thrust, thrust vectoring angle and AOA obtained through solving the trim equations are given in Table 5.

The results show that with increasing flight speed, the required thrust vectoring angle decreases. This was predictable since by pushing aircraft into higher

Table 4. CTUT trim results in near hovering and transition climb flight.

u(km/hr)	Gamma(deg)	Theta(deg)	Required Thrust(N)	Thrust Vector Angle(deg)	AOA(deg)
7	90	89.97	451.2	0	-0.03
18	80	99.25	450.54	-0.2	8.25
36	70	81.07	440.92	-1.05	11.07
54	60	70.06	416.14	-2.43	10.06
72	50	58.9	378.6	-3.98	8.9
90	40	47.27	329.48	-5.84	7.27
108	30	35.84	271.36	-8.2	5.84
126	20	24.63	206.78	-11.67	4.63
144	10	13.61	138.92	-18.08	3.61
216	0	1.11	96.16	-23.67	1.11

Table 5. CTUT trim results in cruise.

u(km/hr)	Required Thrust(N)	Thrust Vector Angle(deg)	AOA(deg)
216	96.16	-23.67	1.11
252	120.52	-17.65	0.55
288	151.24	-13.26	0.18
324	173.76	-10.94	-0.1
450	310.26	-4.82	-0.57
612	571.2	-1.45	-0.79

velocities, the drag also increases, demanding more required thrust. The moment when the cg is produced by this bigger thrust vector is also longer. Therefore, the required thrust vectoring angle to keep the vehicle in trim condition is decreased. Finally, it can be concluded that the aircraft is well trimmable in cruise with acceptable thrust vectoring angles.

PULL-UP TRIM RESULTS

The aircraft arrives in the horizontal to vertical (HTV) transition phase through a pull-up maneuver. In this case, the trim is performed for the beginning of pull-up in different speeds. The required thrust forces are firstly obtained from cruise trim conditions for each considered speed. Then, a pitch rate of 2deg/sec, an average value for this class of UAVs, is set and the thrust vectoring angle, AOA and the pull up radius are calculated. The results are given in Table 6.

The trend of data is similar to those obtained for cruise in terms of thrust vectoring angle and angle of attack. An increase in the required thrust vectoring angle relative to the nonrotating cruise condition is observed. This could be an indication of requirements for more thrust vectoring angles in rotating maneuvers for the current configuration, emphasizing on the fact that some trade-off studies are needed to finalize the aircraft characteristics for satisfying the dynamics requirements.

It should be noted that since the whole study has been carried out longitudinally, no lateral thrust vectoring angle has been used and observed in the presented data. To evaluate the obtained results and the trim algorithm accuracy, CTUT was flown in the previously mentioned computer simulation environment from different trim points as initial conditions. The results are presented in the following sections.

VTH TRANSITION CLIMB SIMULATION

In this case, CTUT is flown from the all VTH transition climb trim conditions obtained in the previous section.

Table 6. CTUT trim results in pull up.

u(km/hr)	Required Thrust(N)	Two Engines T.V Alpha(deg)	AOA(deg)	Pull-up Radius(m)
216	104.3	-28.14	1.56	1718.87
300	168.34	-16.44	0.41	2377.77
360	216.44	-12.56	-0.01	2864.79
432	290.16	-9.18	-0.32	3437.75
504	390.9	-6.54	-0.49	4010.7

Simulations are run for eight seconds in Simulink environment. It is observed that the CTUT flight is stable, however, it tends to gradually rotate downward. This arises mostly because of the numerical error built up due to never perfect trim calculations. In the following, the CTUT trajectory and attitude are shown for the first and eighth trim conditions, Figure 6.

The minus sign of the altitude values is due to the defined direction of height coordinate system which follows the standard NED direction system. Fortunately, the total behavior confirms the validity of the equations and the feasibility of the aircraft in-trim flight regarding the concept of using thrust vectoring for such a vehicle.

CRUISE SIMULATION

Again, CTUT is flown from all cruise trim conditions. Simulations are run for 15 seconds. Regardless of a little tendency to climb because of the previously mentioned numerical errors, the results show very good stability in cruise. Therefore, it can be concluded that a steady state cruise flight in different speeds by using thrust vectoring is feasible for CTUT. The aircraft trajectory and attitude are shown for the first trim condition in Figure 7.

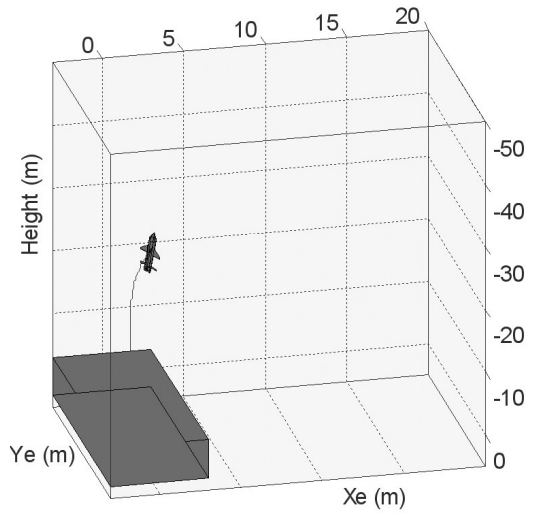

(a) VTH transition climb simulation for the first trim condition.

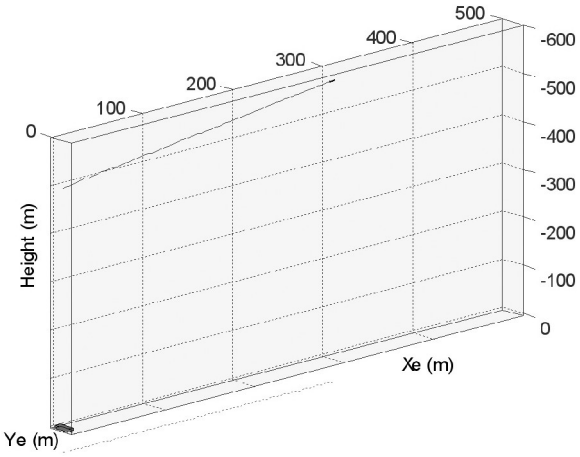

(b) VTH transition climb simulation for the eighth trim condition.

Figure 6. VTH transition climb simulation.

PULL-UP SIMULATION

Finally, CTUT is flown from all pull-up trim conditions, and simulations are run for 15 seconds. The results for the forth trim condition is shown in Figure 8. It is observed that the CTUT could also have a steady flight in pull-up maneuver with an acceptable thrust vectoring angle. This maneuver is used for horizontal to vertical (HTV) transition in the final phase of flight.

ANALYSIS OF THE REQUIRED MASS FLOW RATE

The analysis of required mass flow rate requires complete study of the jet behavior after the nozzle exhaust. The CTUT engine nozzle cross section is circular with an ending divergent Coanda surface over which the secondary jet flows, causing the primary flow to deviate from its normal direction. In this work, a computational fluid dynamics (CFD) approach has been used to study the jet behavior for a fixed geometry. Therefore, the effects of the secondary jet thickness, adding small step over the Coanda surface and geometry of the surface which are the other parameters of concern have not been considered. It should be noticed that the fluidic thrust vectoring analysis is performed in the x-z plane in the direction of vectoring component.

Because of the flow symmetry relative to the x-

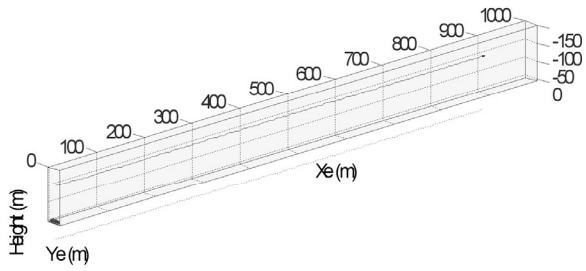

Figure 7. Cruise simulation for the first trim condition.

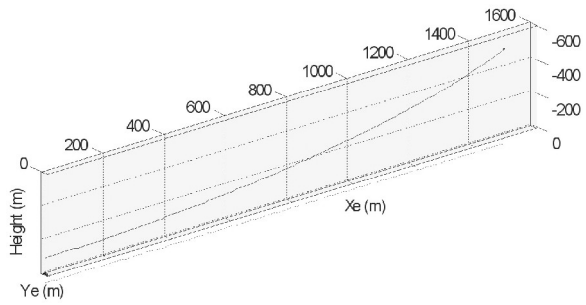

Figure 8. Pull-up simulation for the forth trim condition.

z plane, only half of the geometry of the nozzle has been analyzed. In addition, to produce thrust vectoring in pitch-up direction, a secondary jet flow is assumed in the upper secondary duct around the nozzle casing. The engine exhaust gases and the secondary jet are modelled as mass flows inlet to a control volume with a known ratio assuming that neither varies with thrust vectoring.

The volume in which the nozzle exhaust gases are released has large dimensions compared to the nozzle so that it can obtain the least volume boundaries influence on the jet exhaust. Its boundaries are defined as Velocity Inlet in order to take into account the aircraft velocity, Pressure Outlet and Symmetry, as shown in Figure 9.

A cell centered finite volume technique is used to solve the RANS equations. For these equations, the flow was assumed to be turbulent in all the flow-field.

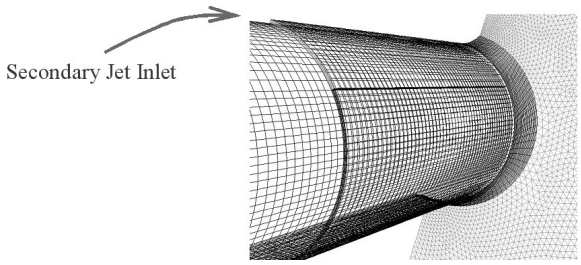

(a) Close-up of nozzle simulation.

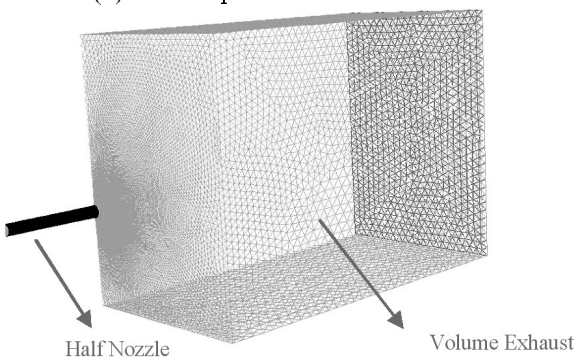

(b) Far-field of nozzle simulation.

Figure 9. Boundary conditions for nozzle simulation.

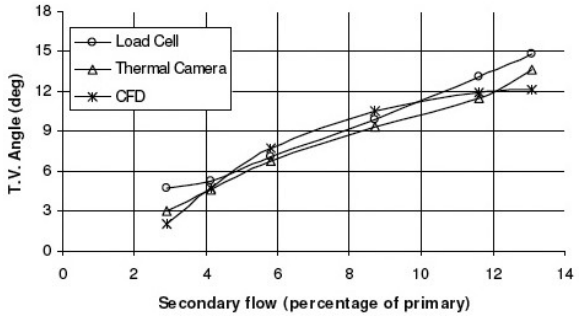

Figure 10. Thrust vector angle vs secondary mass flow for 110000 engine rpm.

The standard K- ϵ model is selected for studying the effects of turbulence in flow. A commercial CFD code has been used as the flow solver [20]. A comprehensive discussion of experimental validation of the results obtained from CFD methods is presented in ref. [21]. In this experimental work, two methods for measurement of thrust vectoring angle were used. The first method was based on using load cells and in the second method a thermal camera was used. The results obtained from both computational and experimental works at 110000 engine rpm is given in Figure 10.

In Figure 11, the required secondary mass flow rate vs. the resulted FTV angle is shown. Using a second order polynomial to fit the data, a relationship can be found between the thrust vectoring angle and the secondary mass flow rate. Referring to the results obtained in the previous sections, the required secondary mass flow rate for each trim condition can be determined. For example, if CTUT cruises at the speed of 288 km/h in a steady state condition, the required mass flow rate would be 13.17 percent of the primary mass flow with a 13.26 degree required thrust vectoring angle. Figure 12 also shows that at very low secondary jet flowing rates i.e. $\dot{m}_s < 0.0112\dot{m}_p$, there is a dead zone in which no thrust vectoring is possible.

Flow simulation has also shown that for high secondary mass flows, fluidic thrust vectoring is more efficient whatever the secondary duct thickness is. At low secondary mass flow rates, the secondary jet separates early from the Coanda surface. If the secondary duct is thick enough, the reverse flow appears whereby the primary jet is vectored in the opposite direction.

It is notable that in the case of using engine bleeding to generate the secondary air jet, the engine performance will be affected. These effects can be easily evaluated using standard turbine performance simulation programs such as the one developed in ref. [22]. In addition, since the total behavior of microjet engines in this category is almost the same, the obtained results can be used for other types of engines as well as for preliminary designs of vectored thrust UAVs.

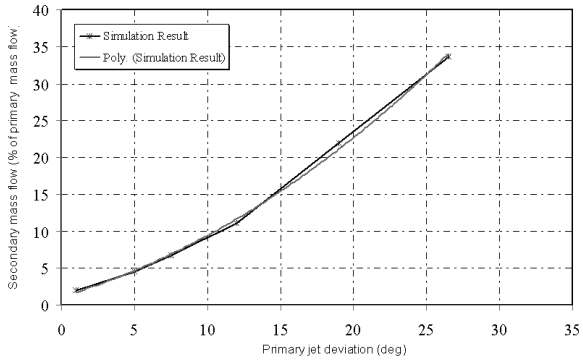

Figure 11. secondary mass flow rate vs thrust vectoring angle,$\dot{m}_S = 0.0251\delta^2_{\text{T.V.}} + 0.5761\delta_{\text{T.V.}} + 1.1203$.

CONCLUSION

In-trim flight of a conceptual fluidic thrust vectored unmanned tail-sitter aircraft has been examined in three major phases of flight. The examination was based on the thrust vectoring angle and the secondary air supply requirements for a longitudinal steady state flight. A six degree of freedom computer simulation with commercially available methods for aerodynamic modeling accompanied by a CFD approach has been used for this analysis. The analysis rendered promising results showing that a steady state flight is feasible over a wide range of flight path angle and speed, using a stand alone Co-flow FTV system with a reasonable and technologically accessible thrust vectoring ability. It should be noted that no trade-off studies has been carried out to date to optimize the configuration characteristics for such a concept. Therefore, it is expected that the results will improve if optimized characteristics were used.

REFERENCES

1. Saghafi F., "Development of a Simulation Tool for Flight Dynamics and Control Investigations of an Articulated VTOL Unmanned Aircraft", Ph.D. Thesis, Cranfield University(1996).
2. Jane's Inc., *Jane's Unmanned Aerial Vehicles and Targets*, Jane's Information Group, (2003).
3. Shephards Inc., *Shephards' Unmanned Vehicles Handbook*, (2005).
4. Hugh Stone R., "The T-Wing Tail-Sitter Research UAV", *AIAA 2002-5970*, Biennial International Powered Lift Conference and Exhibition, Williamsburg, Virginia, (2002).
5. Hugh Stone R., "Aerodynamic Modeling of A Wing in Slipstream Tail-Sitter UAV", *AIAA 2002-5951*, Biennial International Powered Lift Conference and Exhibition, Williamsburg, Virginia, (2002).
6. Quackenbush, T. R., Wachspress, D. A., "Aeromechanical Analysis Tools for Design and Simulation of VTOL UAV Systems", Presented at the American Helicopter Society, 60th annual Forum, Baltimore MD, (2004).
7. Karen A.Deere, "Summary of Fluidic Thrust Vectoring Research Conducted at NASA Langley Research Center", *AIAA 2003-3800*, 21th AIAA Applied Aerodynamics Conference, (2003).
8. Christian Cornell, "Investigation into a Vertical Take off and Landing Concept Witch Uses Fluidic Ejection and the Coanda Effect Coupled with a Vortex / Tornado to Produce Lift", M.Sc. Thesis, Cranfield University(1998).
9. Mark S. Mason, "Fluidic Thrust Vectoring for Low Observable Air Vehicle", 2nd AIAA Flow Control Conference, Portland, Oregon, (2004).
10. Mark S. Mason, "Fluidic Thrust Vectoring for Low Observable Aircraft", CEAS Aerospace Aerodynamic Research Conference, Cambridge, UK, (2002).
11. Lewis R., "The Optimization of A Thrust Vectoring System for A Next Generation Fighter Aircraft", M.Sc. Thesis, Cranfield University(2004).
12. Ransone R., "A photo History of Experimental VS-TOL Aircraft and Their Contributions, AIAAs' X-Planes Symposium", The Westin Hotel Santa Clara, California, (2002).
13. Office of the Secretary of Defense, *Unmanned Aircraft Systems (UAS) Roadmap-2005-2030*, (2005).
14. Scott C. Asbury and Francis J. Capone, "Multiaxis Thrust-Vectoring Characteristics of a Model Representative of the F-18 High-Alpha Research Vehicle at Angles of Attack From 0° to 70°", *NASA Technical Paper 3531*, (1995).
15. Peter H. Zipfel, "Modeling and Simulation of Aerospace Vehicle Dynamics", *AIAA Education Series*, (2000).
16. Brian L. Stevens and Frank L. Lewis, *Aircraft Control and Simulation*, SecondEd., John Wiley & Sons, Inc., (2003).
17. Roskam J., *Airplane Flight Dynamics and Automatic Flight Controls*, Part I and II, Roskam Aviation and Engineering Corporation, (1979).
18. Ing. Holger Friehmelt, "Some Consequences of UAV Design Requirements Specially on UAV Modeling and Simulation", *AIAA 2002-5688*, Modeling and Simulation Technology Conference and Exhibition, Austin, Texas, (2003).
19. Stone R.H, Clarke G., "Optimization of Transition Maneuvers for A Tail-Sitter Unmanned Air Vehicle", Department of Aeronautical Engineering, University of Sydney, Sonacom Pty Ltd, Team Work, (2002).
20. Fluent Inc., *Fluent 6 User Manual*, (2005).
21. Banazadeh A., Saghafi F., Ghoreyshi M., Pilidis P., "Experimental and Computational Investigation of Co-flow Fluidic Thrust Vectoring for a Small Jet Engine", *Aeronautical Journal*, (2006).
22. Cranfield Owned Software, "The Turbomatch Scheme and Performance Calculation for aero/Industrial Gas Turbine", *Cranfield University*, (2004).